Micro-Structured Catalytic Hollow Fibre Reactor for Methane Steam Reforming

Ana Gouveia Gil, Zhentao Wu, David Chadwick, K. Li*[*]

Department of Chemical Engineering, Imperial College London, London SW7 2AZ, United Kingdom

(*)Corresponding authors Tel.: +44 207 5945676; Fax: +44 207 5945629. Email: kang.li@imperial.ac.uk

Abstract

Micro-structured alumina hollow fibres, which contain a plurality of radial micro-channels with significant openings on the inner surface, have been fabricated in this study and used to develop an efficient catalytic hollow fibre reactor. Apart from low mass transfer resistance, a unique structure of this type facilitates the incorporation of Ni-based catalysts, which can be with or without the aged secondary support, SBA-15. In contrast to a fixed bed reactor, the catalytic hollow fibre reactor shows similar methane conversion, with a GHVS of approximately 6.5 times higher, together with a significantly greater CO_2 selectivity and better productivity rates. All these prove the advantages of dispersing catalyst inside the micro-structured hollow fibre together with potentially reducing the quantity of catalysts required.

Keywords: Micro-structured ceramic hollow fibre, Steam methane reforming, Water-gas shift, NiO/SBA-15 catalyst

1 Introduction

Hydrogen has been widely used as a critical feedstock for chemical processes (e.g. petro-chemical and ammonia production) and it is an attractive and promising energy carrier.[1, 2] The state-of-art in hydrogen production is mainly based on steam reforming of fossil fuels, for which methane is preferable due to its availability and high H/C ratio.[1] Water-gas shift reaction can be performed simultaneously in order to produce additional hydrogen, reduce operating costs and facilitate CO_2 capture at the source. The main reactions involved in this process are thus steam reforming (SR) (1) and water-gas shift (WGS) (2), with the overall reaction (3) given below[3, 4]:

$$CH_4 + H_2O \leftrightarrow CO + 3H_2 \qquad \Delta H_{298} = +206.1\ \text{kJ.mol}^{-1} \quad (1)$$

$$CO + H_2O \leftrightarrow CO_2 + H_2 \qquad \Delta H_{298} = -41.15\ \text{kJ.mol}^{-1} \quad (2)$$

$$CH_4 + 2H_2O \leftrightarrow CO_2 + 4H_2 \qquad \Delta H_{298} = +165.0\ \text{kJ.mol}^{-1} \quad (3)$$

Reforming reactions of this type are usually performed in separated catalytic packed-bed reactors (PBRs) due to significant differences in operating temperatures and catalyst composition.[5] The composition and geometry of catalysts for SR and WGS have been extensively studied in order to achieve more efficient heat and mass transfer, lower pressure drop along the reactor and less deactivation due to temperature and concentration profiles. However, the whole process is still energy intensive and costly due to its multi-step character and operating conditions.[6] Process intensification, such as use of micro-reactors, and integration, which combines reaction and product purification into a membrane reactor, can potentially improve the overall efficiency of SRM process. Miniaturization of reaction units, as micro-reactors, have been receiving increasing attention due to their compact design, improved heat and mass transfer efficiencies, reduced weight and enhanced lifetime of catalyst and improved conversion, yield and selectivity.[7-10] All these features come at lower capital and operating costs.[11] The micro-reactor configuration provides mostly a laminar ($1 < Re < 1000$), directed and highly symmetric hydrodynamic flow and reduces the interparticle mass transfer resistance, allowing a better and faster contact between reactants and catalyst.[12, 13] Meanwhile, short diffusion lengths for heat and mass transfer contribute to the small temperature and concentration profiles inside micro-reactors. The precise control of temperature, pressure, residence time and flow rate achieved in micro-reactors reduce the intrinsic risks of performing explosive and highly exothermic reactions. In contrast, PBR

configuration features a turbulent and asymmetric flow with preferential pathways for gases, promoting massive heat and mass transfer resistance and, consequently more significant temperature and concentration profiles.[14]

Ceramic hollow fibres, which can be of a symmetric or asymmetric structure, have been employed as a catalyst substrate for catalytic hollow fibres and catalytic hollow fibre membrane reactors. [15-20] Symmetric hollow fibres (SHF) consist of a fully sponge-like structure with relatively small pore sizes, low porosity and high mass transfer resistance. The incorporation of catalyst into SHF is usually carried out by using a solution technology, such as sol-gel and impregnation, leading to a homogenous distribution of a highly dispersed catalyst. [19, 20] On the other hand, asymmetric hollow fibres (AHF) contain one or more sponge-like layers and a plurality of self-organised micro-voids/channels, which greatly increase the actual surface area to volume ratio over SHF. The catalyst is mainly deposited inside the micro-voids/channels, working as thousands of parallel micro-reactors with enhanced mass and heat transfer efficiency and, consequently, greater catalytic performance. Despite the high surface area to volume ratio, the ceramic hollow fibre normally presents very limited specific surface area. Therefore, secondary supports are usually employed to increase the specific surface area and, as a result, to promote a more uniform distribution of higher loadings of catalyst. [21] Barbara Amorphous 15 (SBA-15) silica emerges as a good secondary support for nickel base catalyst, since it has a high surface area, large pore volume, uniform pore size distribution, thick pore wall and good thermal stability.[22] The nickel particles can be dispersed inside SBA-15 pores and consequently, prevent the sintering of nickel, the metal loss and the formation of large ensembles.[23]

The catalytic performance of catalytic hollow fibres is affected by several factors such as the morphology of the hollow fibre substrate, the distribution and loading of the catalyst, the configuration and operating conditions. Garcia-Garcia et al. [19] investigated the effects of Al_2O_3 hollow fibre morphology on catalyst particle size and on the performance of catalytic membrane reactors for water-gas shift reaction. For this purpose, a Cu-based catalyst was incorporated into symmetric and asymmetric hollow fibres with a sponge-like layer of 300 and 100 µm, respectively, using a sol-gel Pechini method. A uniform catalyst distribution was observed in both symmetric and asymmetric catalytic hollow fibres. However, the particle size of the catalyst presented significant differences; for the symmetric catalytic hollow fibre, a uniform particle size of less than 50 nm was observed throughout the sponge-like layer. On the other hand, the asymmetric catalytic hollow fibre presented catalyst particles of approximately 350 nm and <50 nm in the conical micro-channels region and

sponge-like layer, respectively. The formation of larger particles was caused by the growth of particles during the polymerization step, as the micro-channels were filled with sol-gel solution. In contrast, for the sol-gel solution penetrated into the sponge-like layer by capillarity forces, the volume of solution was too little to allow the growth of the particles. Moreover, it was proved that the catalyst with a smaller particle size presented higher catalytic activity. Furthermore, the enhanced catalytic performance of the asymmetric catalytic hollow fibres is attributed to the improved heat and mass transfer efficiencies and higher internal area provided by the conical micro-channels.

Additionally, the incorporation of catalyst into the conical micro-voids of asymmetric hollow fibres have been proved to significantly reduce the amount of catalyst required for reaction.[24] The micro-voids contribute to higher geometric surface area and, as a result, lead to more uniformly dispersed catalyst. However, previous studies were mainly focused on single reactions, e.g. ethanol steam reforming [17, 25], methanol steam reforming [16, 26] and dehydrogenation reaction [21, 27]. Meanwhile, both ends of the micro-voids are submerged between sponge-like layers with a packed-pore network (average pore size of approximately 0.1-0.2 μm), which limits the methods of incorporating catalysts and is still not ideal for an efficient mass transfer.

As a result, this study addresses the incorporation of Ni-based catalysts, with or without mesoporous SBA-15 as a secondary support, into a micro-structured alumina hollow fibre, forming a highly compact porous reactor for SR and WGS at relatively low operating temperatures (375-550 °C). In contrast to ceramic hollow fibres used previously for similar purposes, the one employed in this study provides a plurality of radial micro-channels, instead of micro-voids, with one end fully open on the inner surface of the hollow fibre. Apart from facilitating the incorporation of catalyst, such micro-channels are more efficient regarding mass transfer. Moreover, the porous reactor of this proof-of-principle study can be considered as an advanced catalytic hollow fibre substrate for further coating of Pd-based membranes, leading to a highly compact membrane reactor design for pre-combustion carbon capture.

2 Experimental

2.1. Preparation of micro-structured Al_2O_3 hollow fibres

The micro-structured Al_2O_3 hollow fibres were prepared by a viscous-fingering induced phase-inversion technique followed by high temperature sintering, allowing great flexibility in morphology control.[28-30] In this study, a uniform ceramic suspension consisting of

approximately 62.7 wt% Al_2O_3 powder (1µm, VWR), 30.6 wt% solvent (dimethyl sulfoxide – DMSO, VWR), 0.4 wt% dispersant (Arlacel P135) and 6.3 wt% polymer binder (polyethersulfone – PESf) was prepared via ball milling. The suspension was then degassed under vacuum to remove air bubbles, transferred into a 200 mL stainless steel syringe and extruded through a tube-in-orifice spinneret (OD 3 mm, ID 1.2 mm) at a rate of 7 $mL \cdot min^{-1}$ into a water bath, with a bore fluid flow rate of 5 $mL \cdot min^{-1}$ and a zero air gap (0 cm). The formed hollow fibre precursors were then dried and sintered at 1300 °C for 4 h (Elite TSH17/75/450).

2.2. Preparation of 25 wt% NiO/SBA-15 catalyst powder

To prepare the SBA-15 sol, 10.0 g of Pluronic P123 (PEG-PPG-PEG block copolymer, average MW = 5800, Aldrich) were firstly dissolved in a mixture of absolute ethanol (50 g, VWR) and hydrochloric acid (2.0 g, 1 M) using a magnetic stirrer (RCT basics, Ika), followed by the addition of 20.8 g of TEOS (tetraethyl orthosilicate, Aldrich). The phase transition of SBA-15 from sol to gel was performed in a fan oven (Salvislab Thermocenter) at 40 °C for 48 h. The SBA-15 gel was then calcinated at 600 °C for 5 h with a heating rate of 1 $°C \cdot min^{-1}$. The powder thus obtained was impregnated with Ni by wet incipient impregnation, using an ethanol based nickel nitrate solution (25wt% Ni), followed by a calcination at 550 °C for 6 h with a heating rate of 1 $°C \cdot min^{-1}$.

2.3. Development of Catalytic Hollow Fibre (CHF)

CHFs were prepared by depositing NiO/SBA-15 catalyst into the micro-structured Al_2O_3 hollow fibre. The catalyst was synthetized in-situ via a two-step process, i.e. incorporation of SBA-15 via a sol-gel method followed by wet impregnation of nickel nitrate.

Incorporation of SBA-15

The SBA-15 sol was prepared as mentioned above. The formulation was heat treated in a fan oven (Salvislab Thermocenter) at 40 °C for 0, 6 and 12 hours to adjust its viscosity, which largely determines the quantity and distribution of SBA-15 inside the Al_2O_3 hollow fibre. The resultant SBA-15 sol was then incorporated into the hollow fibres by immersing the fibres in the SBA-15 precursor solution under vacuum. After expelling the remaining SBA-15 sol inside the hollow fibre lumen, using compressed air, the evaporation of the remaining ethanol (solvent) in the sol was carried out at 40 °C overnight. The fibres were then calcinated at 600 °C for 5 h with a heating rate of 1 $°C \cdot min^{-1}$.

Impregnation of Ni

Ni as the catalytic active phase was incorporated into hollow fibre with or without SBA-15 via impregnation of ethanol based nickel nitrate solution (25 wt% Ni) using the same vacuum assisted process mentioned above. The nickel nitrate was then converted to nickel oxide at 550 °C for 6 h with a heating rate of 1 °C·min^{-1}.

The loadings of SBA-15 and Ni were determined by comparing the weights of the hollow fibres before and after the impregnation and calcination steps. The presence of precursors was taking into account when determining the loadings.

2.4. Characterization

The microstructures of the hollow fibre and CHFs were analysed by scanning electron microscopy (JEOL JSM - 5610LV and LEO Gemini 1525 FEG). Samples were firstly coated with gold in a vacuum chamber for 2 min at 20 mA (EMITECH Model K550) and connected with the metal support by brushing silver paint. A detailed assessment of the pore structure and porosity was carried out by mercury intrusion porosimetry (Autopore IV 9500, Micrometrics), over a pressure range from 1.5x10^3 to 2.3x10^8 Pa and with a set stabilization time of 10 s.

The mechanical strength of the Al_2O_3 hollow fibre was assessed using a tensile tester (Instron Model 5544) with a load cell of 5 kN.

The Brunauer – Emmett – Teller (BET) method was used to investigate the specific surface area of hollow fibres and catalytic hollow fibres. N_2 adsorption isotherms were measured at 77 K using a Tristar 3000 volumetric system. Prior to gas adsorption, samples were degassed at 120 °C overnight and under nitrogen atmosphere.

X-ray diffraction patterns of crushed hollow fibre and CHFs (fine powder) were obtained using an X'celerator detector (X'Pert PRO model), with a radiation source of Cu-Kα, a set voltage of 40 kV, a set current of 40 mA and in a 2Θ degree range from 5 to 80 °.

2.5. Catalytic Performance

Catalytic performance of CHFs was evaluated using the experimental apparatus illustrated in Figure 1. The flow rate of each gas (reactants and inert sweep gas) was controlled by individual mass flow controllers (Brooks Instrument, model 5800) with a collective reader (Brooks Instrument, model 0254). The liquid water was fed into a heating coil (1/16' stainless steel tube) by a syringe pump (Chemix N5000). The temperature of the tubular horizontal

furnace (Vecstar SP HVT) was controlled by temperature controller (CAL 9400) and monitored by a thermocouple located at the central position of the uniform heating zone (7 cm). The inlet and outlet pressure of the reactor were monitored by a digital pressure sensor (Sick, 10bar). The composition of the effluent from the reactor was analysed on-line by a gas chromatograph (Varian 3900) with a packed column (shincarbon, part nbr 19808), after a stabilization time of 1 h at each operating temperature. The total gas flow rate was monitored using a bubble flow meter.

The CHF module was assembled by inserting a 30 cm catalytic hollow fibre into a 3/8' stainless steel tube and sealing both ends with epoxy resin. The module was inserted in the furnace and centred in order to keep the sealed end outside the heating zone. After connecting the module to inlet and outlet streams, the system was purged thoroughly with argon (50 $mL \cdot min^{-1}$) and monitored by oxygen analyser (Model 572 with $\pm 0.01\%$ resolution, Servomex). The reduction of nickel based catalyst was carried out under H_2 atmosphere (10% H_2/Ar of 50 $mL \cdot min^{-1}$) at 400 °C for 2 h. The catalytic performance of the CHFs was investigated at set temperatures between 375 °C and 550 °C, under atmospheric pressure.

For the purpose of comparison, a 25 wt% Ni/SBA-15 catalyst in powder form was also prepared by sol-gel process followed by wet incipient impregnation, and tested in a packed bed reactor (PBR) configuration with a radial dimension of approximately 1 cm. 113 mg of the catalyst were dispersed in 2.00 g of fine silica carbide (SiC), giving a packed-bed length of approximately 2 cm. The quantity of catalyst was defined considering the highest Ni loading achieved for CHFs (27.7 mg of Ni in CHFs of 7 cm). The conditioning and operating procedures adopted were identical to the one described above for CHFs. The catalytic performance at each temperature point was evaluated 3 times, having a deviation of less than 2%."

The overall performance was evaluated based on effective CH_4 conversion (x_{CH_4}), CO_2 selectivity (S_{CO_2}) and productivity rate (Y), which are defined by the equations below:

$$x_{CH_4} = \frac{(F_{CO} + F_{CO_2})}{F_{CH_4\ Inlet}} \times 100\% \quad (eq\ 1)$$

$$S_{CO_2} = \frac{F_{CO_2}}{(F_{CO} + F_{CO_2})} \times 100\% \quad (eq\ 2)$$

$$Y = \frac{(F_{CO} + F_{CO_2})}{m_{Ni}} \quad (eq\ 3)$$

where F_{CH_4}, F_{CO} and F_{CO_2} are the flow rates (mol·min^{-1}) of methane, carbon monoxide and carbon dioxide, respectively, and m_{Ni} is the mass of catalyst in g. Gas hourly space velocity (GHSV) was defined as volumetric flow rate of reactants (m^3·min^{-1}) over total volume of reactor (m^3).

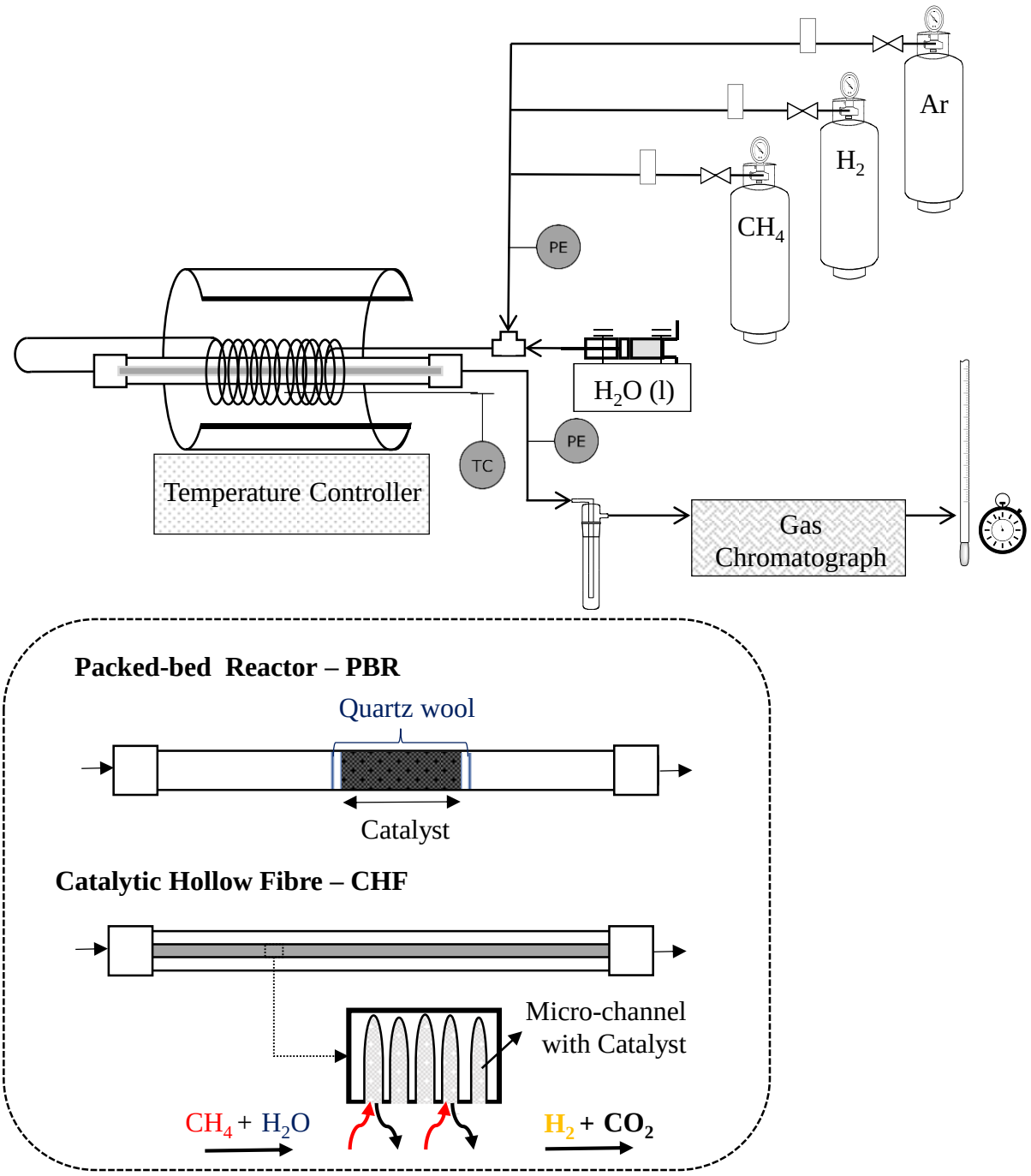

Figure 1. Schematic representation of experimental apparatus.

3 Results and Discussion

3.1 *Micro-structured Alumina Hollow Fibre*

Figure 2 shows the SEM images of Al_2O_3 hollow fibre prepared by a viscous-fingering induced phase-inversion technique and sintered at 1300 °C. The unique asymmetric micro-structured Al_2O_3 hollow fibre consists of two distinct regions: an outer sponge-like layer covering less than 20% of the cross-sectional thickness of the hollow fibre, as can be seen in Figure 2A and A1; and a plurality of self-organised radial micro-channels penetrating through the inner surface, as shown in Figure 2B and B1. Moreover, there is a thin wall separating the radial micro-channels which is part of the sponge-like structure throughout the hollow fibre. The sponge-like structure possesses a packed-pore network, similar to the one of the outer surface as shown in Figures 2C and C1.

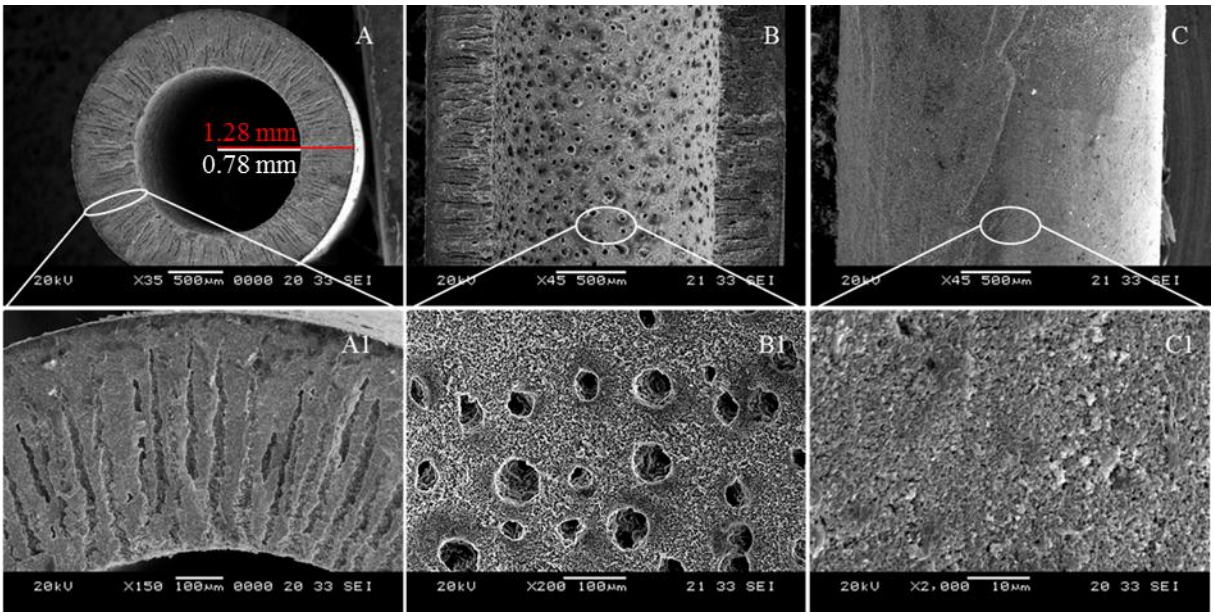

Figure 2. SEM images of Al_2O_3 hollow fibre: (A) cross section; (B) inner surface; and (C) outer surface. (A1), (B1) and (C1) are at a higher magnification of (A), (B) and (C), respectively.

Figure 3 provides further details of the asymmetric pore structure of the alumina hollow fibre. As can be seen, the lower and wider peak from 5 to 25 μm represents the radial micro-channels and the second peak at approximately 0.18 μm represents the average pore size of the sponge-like structure, agreeing well with previous studies.[30]

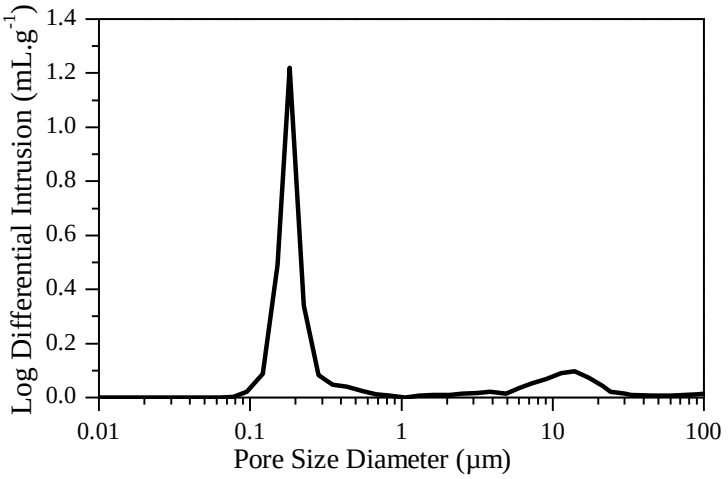

Figure 3. Mercury intrusion porosimetry of Al_2O_3 hollow fibre.

The properties of the sponge-like structure, such as thickness, porosity and pore size, largely determine the mechanical strength and mass transfer across and inside the fibre. Usually, a higher sintering temperature leads to better mechanical strength, but at the expense of lower porosity and higher mass transfer resistance. The mechanical strength of such fibres is approximately 56 MPa, which is 34% higher than reported in a previous study using fibres made of the same material, with similar morphology and sintered at the same temperature.[30] The higher mechanical strength might be caused by a slight difference in the thickness of the outer sponge-like layer, as well as number and dimension of the radial micro-channels.

The large number of radial micro-channels inside the hollow fibre contributes to significantly increase the geometric surface area, to ease catalyst incorporation and to improve interaction between reactants and catalyst. The high porosity of the hollow fibre (57%), which is provided not only by the large number of micro-channels, but also by the interparticle spaces inside the sponge-like structure, significantly reduces mass transfer resistance. Garcia-Garcia et al[16] investigated the application of asymmetric Al_2O_3 hollow fibres for catalytic reactions. The asymmetric Al_2O_3 hollow fibre, with 50MPa of mechanical strength and a nitrogen permeation of 200 $L \cdot m^{-2} \cdot s^{-1}$ at 200KPa, was used as a support for a palladium membrane and as a substrate for a copper based catalyst. Despite the significant length (approximately 80% of cross-section) of petal shaped micro-voids, a hollow fibre of this type still represents a considerable barrier to mass transfer, mainly due to its lower overall porosity and much less porous inner surface. In contrast, the highly porous micro-structured hollow fibre in this

study presents a high nitrogen permeability of 425 $L \cdot m^{-2} \cdot s^{-1}$, measured at room temperature, 200kPa and with a membrane area of 0.8 cm^2. This highlights the low mass transfer resistance of the substrate, which will greatly promote the contact between reactants and catalyst. Moreover, the dimensions and volume of the radial micro-channels play an important role in catalyst deposition and loading, especially for catalyst wash coating where the size of catalyst particles is suggested to be at least three times smaller than the micro-channel entrances. [16, 29] On the other hand, incorporating catalyst via a solution technique, such as depositing the secondary support via a sol-gel based method followed by impregnating the catalytic active phase, has been proved efficiently for both symmetric and asymmetric ceramic hollow fibre supports. [15, 16] While due to the less porous surface of the previous hollow fibre substrates, concentration and viscosity of the precursor solutions need to be carefully controlled to avoid blocking the surface that can increase mass transfer resistance, thus limited the quantity of catalyst that can be deposited. Benefit from the large micro-channel openings, more concentrated precursor solutions can thus be employed for higher loadings of the secondary support as well as the catalyst active phase, without affecting the mass transfer efficiency of the hollow fibre substrates.

3.2 *Catalytic Hollow Fibre*

Incorporation of SBA-15

The overall performance of catalytic reactors for methane reforming reactions is greatly affected by the specific surface area provided by the substrate in which the active metal, nickel, is deposited.[21] Secondary supports, such as SBA-15, are commonly required in order to provide additional surface area and, consequently, reduce the deactivation of metal based catalyst due to carbon formation and sintering. After high temperature sintering, the specific surface area of the alumina hollow fibre is considerably low. As a result, SBA-15 was incorporated prior to impregnation of catalytic phase. The deposition of SBA-15 was performed by a sol-gel based process since this technique has been widely used for incorporation of catalyst into hollow fibre and it can virtually be used in any type of micro-structured support [20]. The quantity and distribution of SBA-15 inside the micro-structured Al_2O_3 hollow fibre affects both Ni impregnation and catalytic performance, and can be controlled by varying the ageing time and hence the viscosity of the SBA-15 sol. Table 1 and Figure 4 show the properties and SEM images of the hollow fibres without and with SBA-15 at different ageing times. SBA-15 loadings of 2.61%, 5.84% and 7.27% were obtained for the ageing time of 0 hour, 6 hours and 12 hours, respectively, which is reasonable since the adhesion of sols to a porous substrate increase with viscosity.[31] The incorporation of SBA-15

into hollow fibres largely enhanced the specific surface area by 6, 13 and 19 times for the ageing time of 0 hour, 6 hours and 12 hours, respectively. These results are in agreement with a previous study.[21] Apart from increasing the specific surface area, ageing time affected the distribution of SBA-15 inside the hollow fibre. Thus can be seen in Figure 4 A1-D1, with longer ageing time, and consequently more viscous SBA-15 sol, the penetration of SBA-15 sol into the packed-pore network of the sponge-like structure is more difficult. As a result, the SBA-15 is preferentially distributed along the micro-channels, as shown in Figure 4 A2-D2, and it covers more small pores on the inner surface (packed-pore network) among micro-channel entrances, as can be seen in Figure 4 A3-D3. Moreover, the incorporation of SBA-15, for all ageing time sols, did not block, fully or partially, the micro-channels entrances on the inner surface of the fibre.

Table 1. Loading and specific surface area of different ageing time SBA-15/ Al_2O_3 HF.

Composition of CHF	SBA-15 Loading (wt %)	Specific Surface Area ($m^2.g^{-1}$)
Al_2O_3 HF	n/a	2.6
0h SBA-15	2.61	14.8
6h SBA-15	5.84	34.4
12h SBA-15	7.27	50.1

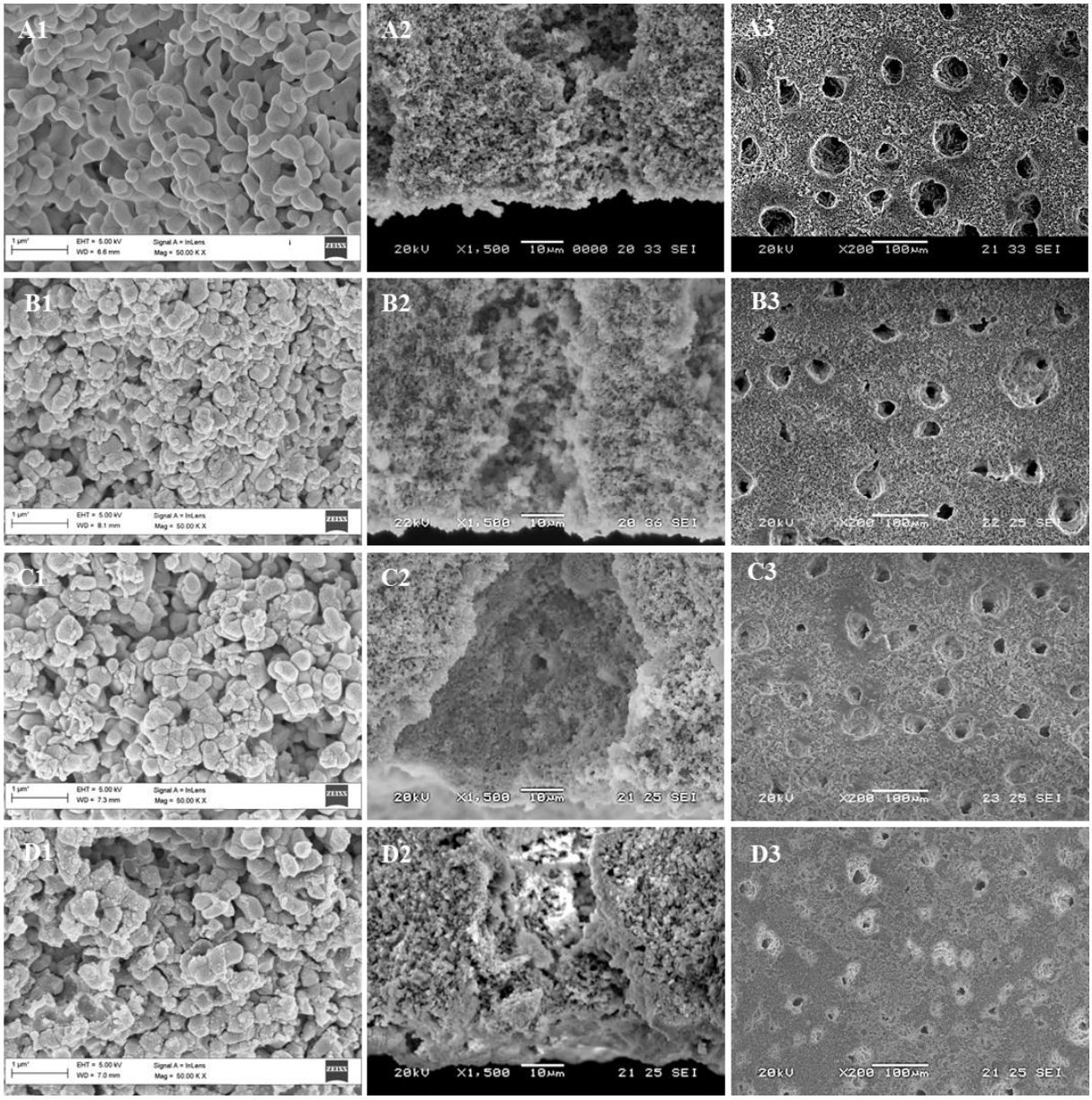

Figure 4. SEM images of Al_2O_3 hollow fibre (A) and SBA-15 in Al_2O_3 hollow fibre with ageing time of 0h (B), 6h (C) and 12h(D): A1, B1,C1 and D1 sponge-like layer between micro-channels; A2, B2, C2 and D2 micro-channel entrance; and A3, B3, C3 and D3 inner surface.

Wet Impregnation of Ni

The nickel nitrate, precursor of catalytic active nickel, was successfully impregnated into the Al_2O_3 hollow fibres with or without SBA-15. As can be seen in Figure 5, crystals of nickel oxide were formed along the radial micro-channels of all the samples; however neither crystal nor particles of NiO could be clearly identified in SEM images of sponge-like structure. Despite this fact, a homogeneous distribution of NiO on the packed-pore structure was visually observed by a light grey colour, as shown in Figure 6. Although the adsorption

capacity of SBA-15 is significantly higher than alumina, the actual loading of NiO in the samples with and without SBA-15 was quite similar (varying from 4 to 5.7 wt% and determined by weight difference). This is mainly because the amount of SBA-15 incorporated is considerably small (Table 1), when compared with the significant pore volume from both radial micro-channels and sponge-like structure of the alumina hollow fibre.

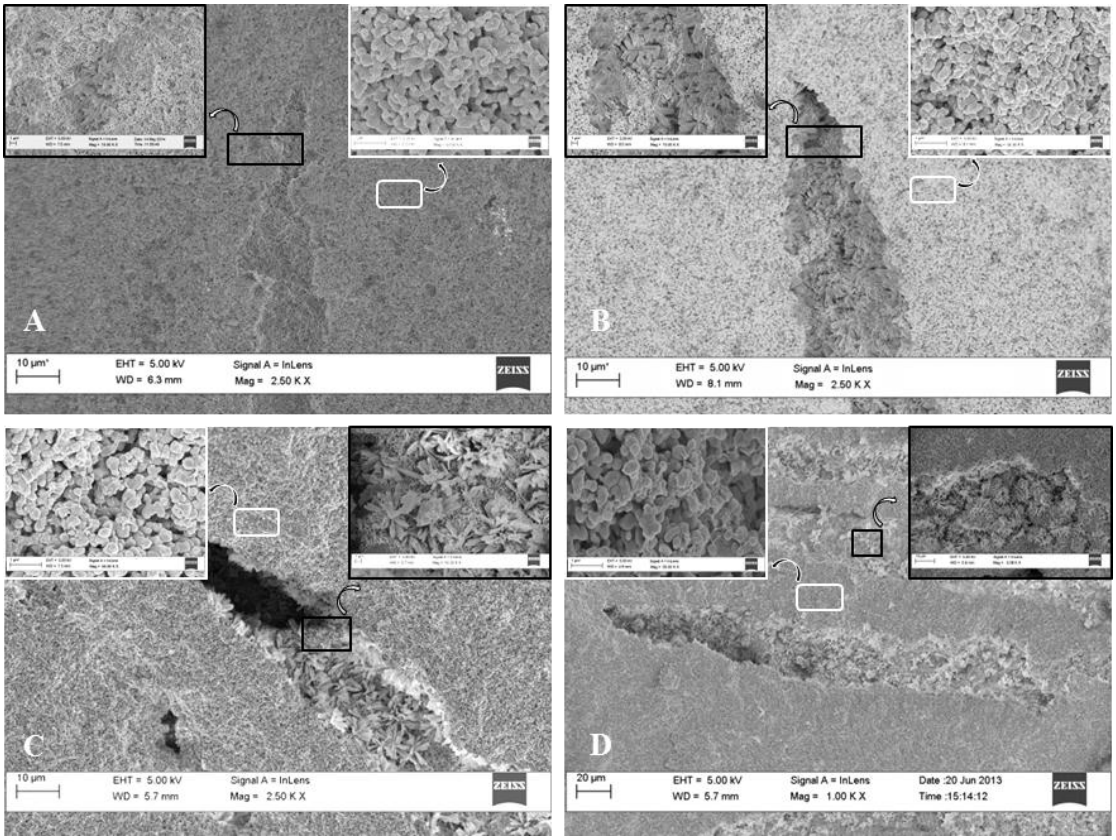

Figure 5. SEM images of: (A) NiO/Al_2O_3 HF, (B) NiO/0h SBA-15 - CHF, (C) NiO/6h SBA-15 - CHF and NiO/12h SBA-15 – CHF.

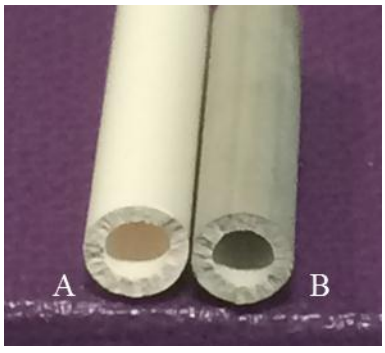

Figure 6. Image of Al_2O_3 hollow fibre (A) and NiO/12h SBA-15 – CHF (B).

The X-ray diffraction patterns of the CHFs and pure Al_2O_3 hollow fibre are presented in Figure 7. The distinctive peaks of Al_2O_3 and NiO can be identified in all CHF samples. However, the intensity of the NiO peaks was low due to the reduced amount and highly dispersion. Furthermore, the amorphous nature and the small quantity of the SBA-15 unable the detection of the characteristic peak of SBA-15 at 2θ value of 21.79°.

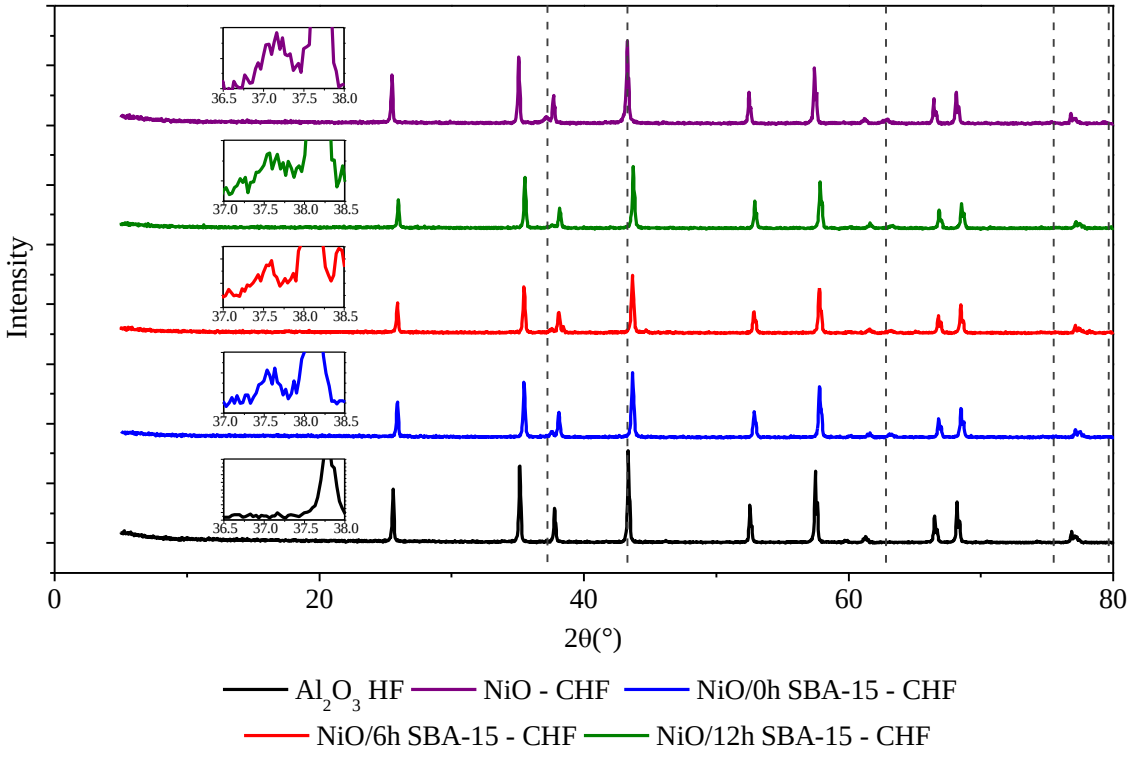

Figure 7. XRD patterns of assembled CHFs and Al_2O_3 HF and --- NiO characteristic peaks.

The porosity of the hollow fibre was considerably affected by the incorporation of NiO or NiO&SBA-15, as can be seen in Table 2. A porosity loss of 3.7, 16.5, 24.1, 24.3% was observed for NiO, NiO/0h SBA-15, NiO/6h SBA-15 and NiO/12h SBA-15 – CHFs, respectively.

Table 2. Mass of nickel available for reaction and porosity of the substrate after catalyst incorporation.

Reactor Configuration	Mass of Ni (mg)	Porosity (%)
PBR	27.7	n/a
Ni – CHF	27.7	54.4
Ni/0hSBA-15 – CHF	19.6	47.2
Ni/6hSBA-15 – CHF	16.7	43.9
Ni/12hSBA-15 – CHF	23.4	43.2

Figure 8 shows a more detailed analysis on the pore structure and reveals that the radial micro-channels (between 5 and 25 µm) are little affected by the incorporation of NiO and SBA-15, which is in agreement with Figure 4 and Figure 5. In contrast, the pore size of the sponge-like structure was highly affected due to the partial filling of the interparticles spaces. As the ageing time of SBA-15 increases, the intensity of the peak at 0.18 µm decreases and a third peak, with smaller diameter (0.07 µm), becomes more manifest and intense. The deposition of SBA-15 particles in the packed-pore structure and formation of SBA-15 layer along the micro-channels resulted in the partial filling and blockage of pores and, consequently, a reduction of their size. As shown in Figure 4B1 and B2, the majority of the SBA-15 incorporated in 0h SBA-15 CHF was distributed in the interparticles spaces of the packed pore sponge-like structure, leading to a reduction of the overall porosity in the sponge-like structure. This statement is supported by mercury intrusion porosimetry results, in which the peak corresponding to packed pore structure suffered a small drop in intensity and slight shift in position towards a smaller pore size. Such phenomenon becomes more significant with SBA-15 aged at longer time due to the formation of a SBA-15 layer along the micro-channel.

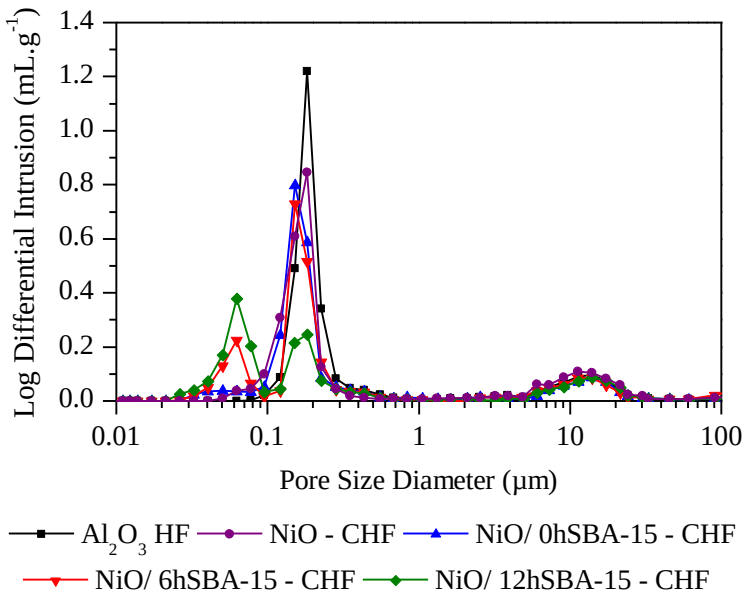

Figure 8. MIP results of the Al_2O_3 HF and different catalytic hollow fibres.

3.3 *Catalytic Performance*

The catalytic performance of the CHFs and 25wt%NiO/SBA-15 catalyst was evaluated based on effective methane conversion, CO_2 selectivity and productivity rate presented in Figure 9. Table 2 lists the amount of Ni (mg) involved in the different reactors.

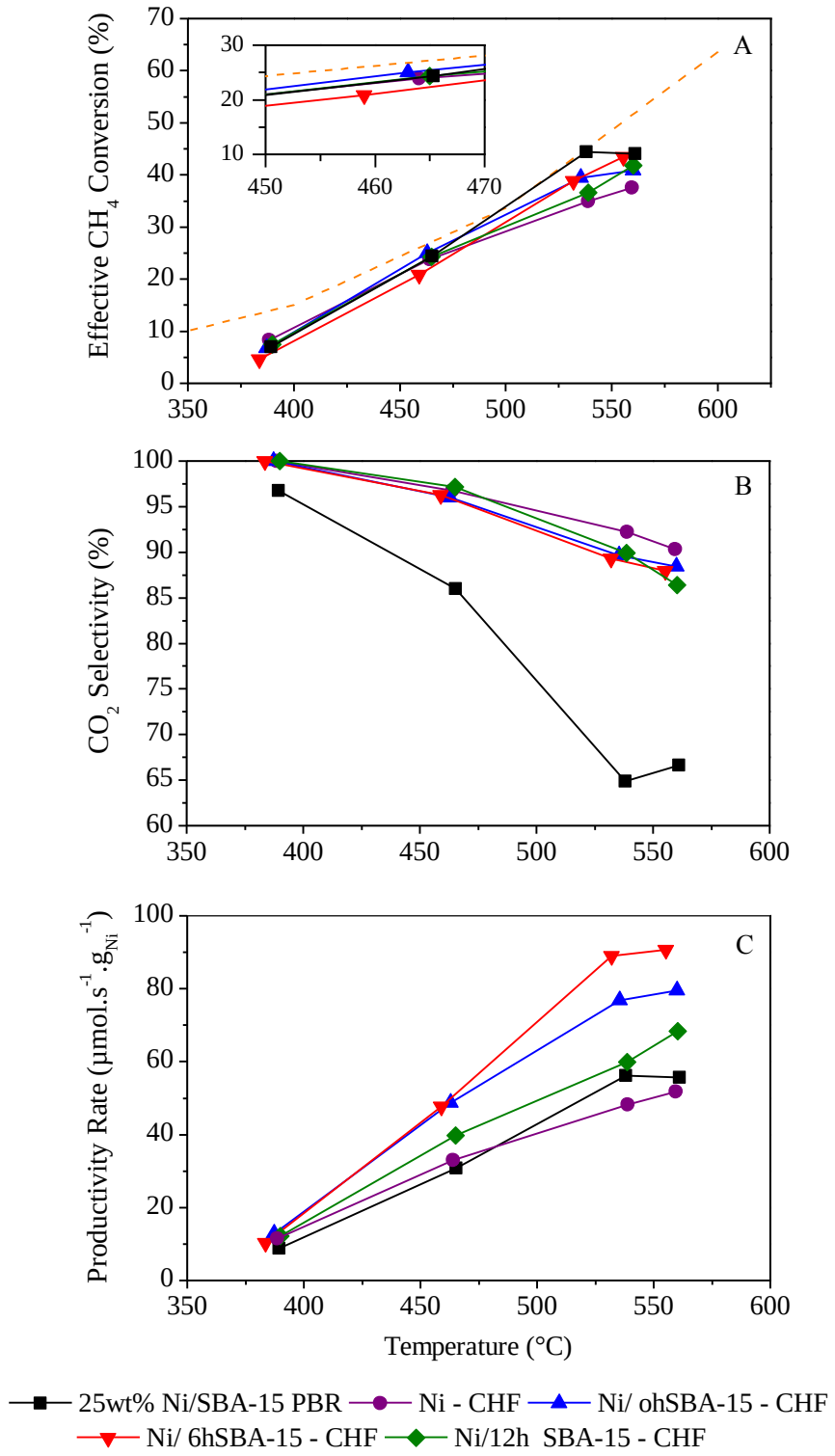

Figure 9. Temperature dependent (A) effective methane conversion, (B) CO_2 selectivity and (C) productivity rate of different CHFs and PBR configurations.

Figure 9A shows the methane conversion of CHFs and PBR as function of temperature. Apparently, effective methane conversion for both CHFs and PBR increase with temperature showing similar trends among all different configurations and reaching values close to the equilibrium conversion. Although the methane conversion of PBR is slightly higher than that of CHFs at 540 °C, it started to drop in a slow manner at approximately 560 °C. This may be caused by encapsulation of nickel due to instability of SBA-15 structure, as reported by McMinn et al[3232]. In contrast, such drop in methane conversion was not observed in CHFs. One of the possible reasons is that CHFs provide an ideal flow of the reactants, with the widely opened radial micro-channels significantly reducing mass and heat transfer resistance, and consequently allowing a more efficient interaction between the reactants and the catalyst. At temperature of 465°C, the effective methane conversion of all CHFs, including CHF without SBA-15 (Ni – CHF), is rather close to the thermodynamic equilibrium. This indicates great efficiencies when dispersing catalyst inside the micro-structured alumina hollow fibre. On the other hand, at elevated operating temperatures (>500°C), CHFs containing SBA-15 showed higher methane conversion over the Ni-CHF, which may be linked to the additional surface area provided by SBA-15. As the operating temperature increases and reaches values similar or above catalyst calcination temperature (540 °C), the difference between actual methane conversion and thermodynamic equilibrium value increases, possibly as a result of sintering of the catalyst, loss of active sites and encapsulation of Ni by both SBA-15 and Al_2O_3. [32]

Figure 9B compares CO_2 selectivity of different reactor designs. CO_2 selectivity keeps decreasing with the increasing operating temperatures, as expected from the thermodynamic point of view, since SMR is highly endothermic and WGS is slightly exothermic. Evidently, CO_2 selectivity of PBR is much lower than the CHFs counterparts within the selected range of operating temperatures. The benefits of dispersing catalyst inside micro-structured alumina hollow fibres are then further proved to enhance reaction performance by reducing mass transfer resistance and, consequently, achieving a more uniform concentration profile. A uniform and highly dispersed catalyst also increases the accessibility of the catalyst to reactants, which increase the possibility of CO (produced in SMR) to be further converted into CO_2 via WGS.

Due to major differences on reactor configuration, such as flow patterns, catalyst distribution and loading, reactor volume and contact/residence time, the overall performance of the different reactor configurations cannot be precisely assessed by exclusively analysing

effective methane conversion and CO_2 selectivity. Although the methane conversions are quite similar, the nickel loading is considerably different and gas hourly space velocity (GHVS) in CHF is approximately 6.5 times higher than in PBR configuration, 27255h^{-1} and 4053h^{-1}, respectively. Consequently, productivity rate, which is calculated based on the formation of CO and CO_2 over the mass of Ni involved in each reactor configuration (eq 3), is employed for a more sensible comparison. As seen in Figure 9C, the productivity rate of CHFs can be much greater than PBR. However, at intermediate temperatures the effective methane conversion of PBR is rather close to thermodynamic equilibrium value and, as a result, it is not clear if the catalyst is operating at full capacity. Therefore, the comparison between catalytic performance of CHFs and PBR must be assessed at temperature of 540°C. The productivity rate of PBR is considerably lower than CHFs containing SBA-15, which can be an advantage of dispersing catalyst inside the micro-structured hollow fibres. The discrepancy between the CHFs with SBA-15 might be due to the difference of actual mass of Ni, as the effective methane conversion values are very similar. This suggests the amount of nickel available is higher than necessary and requires further tuning.

4 Conclusions

A micro-structured catalytic hollow fibre was successfully developed by incorporating Ni/SBA-15 catalyst into alumina hollow fibres with low mass and heat transfer resistance. The unique and widely opened radial micro-channels (5-25μm) on the inner surface of hollow fibre facilitate catalyst incorporation and contribute to higher interaction between the reactants and catalyst, resulting in a higher catalytic performance. The methane conversion achieved from both CHF and PBR configuration was similar and close to thermodynamic equilibrium values (around 25% at 465°C); however, the space velocity in CHF was considerably higher (approximately 6.5 times). Meanwhile, greater CO_2 selectivity was obtained from CHFs, due to a more uniform concentration and temperature profiles when comparing to PBR. Furthermore, the great productivity rate of CHFs containing SBA-15 indicates their potential in further reducing the catalyst required.

Acknowledgements

The authors gratefully acknowledge the research funding provided by EPSRC in the United Kingdom (Grant nos.: EP/ I010947/1)

References

(1) Angeli, S. D.; Monteleone, G.; Giaconia, A.; Lemonidou, A. A. State-of-the-art catalysts for CH4 steam reforming at low temperature. *Int. J. Hydrogen Energy* **2014,** 39, (5), 1979-1997.

(2) Chaubey, R.; Sahu, S.; James, O. O.; Maity, S. A review on development of industrial processes and emerging techniques for production of hydrogen from renewable and sustainable sources. *Renew. Sust. Energ. Rev.* **2013,** 23, (0), 443-462.

(3) Holladay, J. D.; Hu, J.; King, D. L.; Wang, Y. An overview of hydrogen production technologies. *Catal. Today* **2009,** 139, (4), 244-260.

(4) Liu, K.; Song, C.; Subramani, V. *Hydrogen and Syngas Production and Purification Technologies*. *Wiley* **2009**.

(5) Mendes, D.; Mendes, A.; Madeira, L. M.; Iulianelli, A.; Sousa, J. M.; Basile, A. The water-gas shift reaction: from conventional catalytic systems to Pd-based membrane reactors—a review. *Asia-Pac. J. Chem. Eng.* **2010,** 5, (1), 111-137.

(6) Aasberg-Petersen, K.; Nielsen, C. S.; Jørgensen, S. L. Membrane reforming for hydrogen. *Catal. Today* **1998,** 46, (2–3), 193-201.

(7) Tonkovich, A. L. Y.; Yang, B.; Perry, S. T.; Fitzgerald, S. P.; Wang, Y. From seconds to milliseconds to microseconds through tailored microchannel reactor design of a steam methane reformer. *Catal. Today* **2007,** 120, (1), 21-29.

(8) Tonkovich, A. Y.; Perry, S.; Wang, Y.; Qiu, D.; LaPlante, T.; Rogers, W. A. Microchannel process technology for compact methane steam reforming. *Chem. Eng. Sci.* **2004,** 59, (22–23), 4819-4824.

(9) Zanfir, M.; Gavriilidis, A. Catalytic combustion assisted methane steam reforming in a catalytic plate reactor. *Chem. Eng. Sci.* **2003,** 58, (17), 3947-3960.

(10) Zhai, X.; Ding, S.; Cheng, Y.; Jin, Y.; Cheng, Y. CFD simulation with detailed chemistry of steam reforming of methane for hydrogen production in an integrated micro-reactor. *Int. J. Hydrogen Energy* **2010,** 35, (11), 5383-5392.

(11) Charpentier, J. C. Process Intensification by Miniaturization. *Chem. Eng. Technol.* **2005,** 28, (3), 255-258.

(12) Jähnisch, K.; Hessel, V.; Löwe, H.; Baerns, M. Chemistry in Microstructured Reactors. *Angew. Chem. Int. Ed.* **2004,** 43, (4), 406-446.

(13) Kolb, G.; Hessel, V. Micro-structured reactors for gas phase reactions. *Chem. Eng. J* **2004,** 98, (1–2), 1-38.

(14) Wang, F.; Qi, B.; Wang, G.; Li, L. Methane steam reforming: Kinetics and modeling over coating catalyst in micro-channel reactor. *Int. J. Hydrogen Energy* **2013,** 38, (14), 5693-5704.

(15) García-García, F. R.; Rahman, M. A.; Kingsbury, B. F. K.; Li, K. A novel catalytic membrane microreactor for COx free H2 production. *Catal. Commun.* **2010,** 12, (3), 161-164.

(16) García-García, F. R.; Kingsbury, B. F. K.; Rahman, M. A.; Li, K. Asymmetric ceramic hollow fibres applied in heterogeneous catalytic gas phase reactions. *Catal. Today* **2012,** 193, (1), 20-30.

(17) Rahman, M. A.; García-García, F. R.; Li, K. Development of a catalytic hollow fibre membrane microreactor as a microreformer unit for automotive application. *J. Membr. Sci.* **2012,** 390-391, 68-75.

(18) García-García, F. R.; Torrente-Murciano, L.; Chadwick, D.; Li, K. Hollow fibre membrane reactors for high H2 yields in the WGS reaction. *J. Membr. Sci.* **2012,** 405–406, (0), 30-37.

(19) García-García, F. R.; Li, K. New catalytic reactors prepared from symmetric and asymmetric ceramic hollow fibres. *Appl. Catal., A: General* **2013,** 456, (0), 1-10.

(20) Gallegos-Suárez, E.; García-García, F. R.; González-Jiménez, I. D.; Rodríguez-Ramos, I.; Guerreo-Ruiz, A.; Li, K. Ceramic hollow fibres catalytic enhanced reactors for glycerol steam reforming. *Catal. Today* **2014,** 233, (0), 21-30.

(21) Gbenedio, E.; Wu, Z.; Hatim, I.; Kingsbury, B. F. K.; Li, K. A multifunctional Pd/alumina hollow fibre membrane reactor for propane dehydrogenation. *Catal. Today* **2010,** 156, (3–4), 93-99.

(22) Zhao, D.; Sun, J.; Li, Q.; Stucky, G. D. Morphological Control of Highly Ordered Mesoporous Silica SBA-15. *Chem. Mat.* **2000,** 12, (2), 275-279.

(23) Wan, H.; Li, X.; Ji, S.; Huang, B.; Wang, K.; Li, C. Effect of Ni Loading and CexZri-xO2 Promoter on Ni-Based SBA-15 Catalysts for Steam Reforming of Methane. *J. Nat. Gas. Chem.* **2007,** 16, (2), 139-147.
(24) Rahman, M. A.; García-García, F. R.; Hatim, M. D. I.; Kingsbury, B. F. K.; Li, K. Development of a catalytic hollow fibre membrane micro-reactor for high purity H2 production. *J. Membr. Sci.* **2011,** 368, (1–2), 116-123.
(25) Rahman, M. A.; García-García, F. R.; Li, K. On-board H2 generation by a catalytic hollow fibre microreactor for portable device applications. *Catal. Commun.* **2011,** 16, (1), 128-132.
(26) García-García, F. R.; Tsang, S. C.; Li, K. Hollow fibre based reactors for an enhanced H2 production by methanol steam reforming. *J. Membr. Sci.* **2014,** 455, (0), 92-102.
(27) Hatim, M. D. I.; Fazara, M. A. U.; Syarhabil, A. M.; Riduwan, F. Catalytic Dehydrogenation of Methylcyclohexane (MCH) to Toluene in a Palladium/Alumina Hollow Fibre Membrane Reactor. *Procedia Engineering* **2013,** 53, (0), 71-80.
(28) Kingsbury, B. F. K.; Li, K. A morphological study of ceramic hollow fibre membranes. *J. Membr. Sci.* **2009,** 328, (1-2), 134-140.
(29) Kingsbury, B. F. K.; Wu, Z.; Li, K. A morphological study of ceramic hollow fibre membranes: A perspective on multifunctional catalytic membrane reactors. *Catal. Today* **2010,** 156, (3–4), 306-315.
(30) Lee, M.; Wu, Z.; Wang, R.; Li, K. Micro-structured alumina hollow fibre membranes – Potential applications in wastewater treatment. *J. Membr. Sci.* **2014,** 461, (0), 39-48.
(31) Chen, K.-Y.; Shen, C.-C.; Lee, C.-Y.; Lee, S.-J.; Leu, C.-H.; Wang, J.-H.; Yeh, C.-T. Coating powdered copper catalyst with yttria sol. *Mater. Chem. Phys.* **2011,** 128, (1–2), 57-61.
(32) McMinn, T. E.; Moates, F. C.; Richardson, J. T. Catalytic steam reforming of chlorocarbons: catalyst deactivation. *Appl. Catal., B: Environmental* **2001,** 31, (2), 93-105.